



# Onset Time of the GLE 72 Observed at Neutron Monitors and its Relation to Electromagnetic Emissions

V. Kurt<sup>1</sup> · A. Belov<sup>2</sup> · K. Kudela<sup>3,4</sup> · H. Mavromichalaki<sup>5</sup> ·  
L. Kashapova<sup>6</sup> · B. Yushkov<sup>1</sup> · C. Sgouropoulos<sup>5</sup>

Received: 24 September 2018 / Accepted: 21 January 2019  
© Springer Nature B.V. 2019

**Abstract** We present an overview of the ground-level enhancement (GLE 72) of the cosmic-ray intensity associated with the recent powerful solar flare SOL2017-09-10 (X-ray class X8.9) based on the available neutron monitor (NM) network observations and on data from the satellite GOES 13. The maximum increase at high-latitude near-sea-level NMs was  $\approx 6-7\%$  (2-min averages), greater with better time resolution. A scatter plot of the maximum increase of the GLE *versus* solar energetic-particle (SEP, proton) flux  $> 100$  MeV shows one of the softest spectra among GLEs relative to the SEP fluxes. However, at two high-mountain middle-latitude NMs the increase was  $\approx 1\%$ , indicating the possibility of proton acceleration up to 6 GeV. Among the analyzed NM data the Fort Smith (FSMT) NM shows the earliest and the rather high increase between 16:06–16:08 UT. This indicates an anisotropy in the first phase of the GLE event. We calculate the acceptance cones of several NM stations at high latitudes and contours of pitch angles corresponding to the interplanetary magnetic field (IMF). When employing the available data we find that pion-decay  $\gamma$ -ray emission onset is in accordance with the time of the main flare energy release. The observed time interval of the impulsive burst of  $> 100$  MeV  $\gamma$ -ray emission probably corresponds to the time of a turbulent current sheet creation. The observed location of the impulsive burst pion-decay emission source coincides with the active region and the cusp-shaped structure. It seems that models assuming sub-relativistic proton production beginning in a turbulent reconnecting current sheet are consistent with the observations. If these particles were released

---

✉ H. Mavromichalaki  
[emavromi@phys.uoa.gr](mailto:emavromi@phys.uoa.gr)

<sup>1</sup> Skobeltsyn Institute of Nuclear Physics, Lomonosov Moscow State University, Moscow, 119991, Russian Federation

<sup>2</sup> IZMIRAN, Troitsk, Moscow region, 142190, Russian Federation

<sup>3</sup> Nuclear Physics Institute, Czech Academy of Sciences, Řež, Czech Republic

<sup>4</sup> Institute of Experimental Physics, Slovak Academy of Sciences, Košice, Slovakia

<sup>5</sup> Nuclear and Particle Physics Department, Faculty of Physics, National and Kapodistrian University of Athens, 15784 Athens, Greece

<sup>6</sup> Institute of Solar-Terrestrial Physics, Russian Academy of Sciences, Irkutsk, 664033, Russian Federation

from the Sun during a type III emission with a pion-decay maximum at  $16:00:30 \pm 30$  UT, we get a plausible path length equal to  $1.5 \pm 0.3$  AU of the particles responsible for the onset of the SEP event and GLE. The time lag of GLE 72 corresponds to the most probable interval of the time difference between GLE onset and main flare energy release. Although other scenarios are not excluded we attribute the protons that create the pion-decay emission and the protons responsible for the GLE and SEP event onset to a general population of accelerated particles.

**Keywords** Solar flares, solar energetic particles, cosmic-ray intensity, neutron monitors, ground-level enhancements

## 1. Introduction

Ground-level enhancements (GLEs) have been observed since a long time, most probably since the events of 28 February and 7 March 1942, when they were identified by Forbush (1946), and named later GLE 1 and GLE 2, respectively. Reviews on solar proton events (SPEs) and GLEs can be found, *e.g.*, in Shea and Smart (1990), Moraal and McCracken (2012). The GLEs, which are also important for radiation dosage at airplane altitudes, are analyzed according to the data of the neutron monitor (NM) network (*e.g.* Bütikofer and Flücker, 2009; Mishev, Poluianov, and Usoskin, 2017; Mishev *et al.*, 2018; Copeland, Matthiä, and Meier, 2018; Mishev and Usoskin, 2018). Radiation hazard alerts are based also on NM data if they are available in real time with high resolution (*e.g.* Souvatzoglou *et al.*, 2014; Mavromichalaki *et al.*, 2018). The high resolution database of real-time neutron monitor measurements (NMDB) is accessible at [www.nmdb.eu](http://www.nmdb.eu) and is described by Mavromichalaki *et al.* (2011). During the systematic investigation of GLEs, a number of 72 events were recorded till now (Belov *et al.*, 2010; Miroshnichenko, 2015; Poluianov *et al.*, 2017). A database of GLEs has been developed over the years by the international scientific community (Shea *et al.*, 2001; Duldig and Watts, 2001, and the references therein). Recently the database including all GLEs was moved to the University of Oulu (<http://cosmicrays oulu.fi/>).

There is no doubt that each GLE is connected with powerful solar eruptive events, but it is still debated whether protons responsible for the beginning of GLEs and high-energy solar energetic-particles (SEPs) are accelerated just directly during the flare energy release or when a shock wave created by a coronal mass ejection (CME) propagates in the upper corona (Reames, 2009a, 2009b).

A substantial argument when choosing a scenario is the pion-decay emission observations. Pion-decay emission occurrence during a solar eruptive event ascertains the proton acceleration up to high energies ( $> 300$  MeV) and their interaction with the dense solar atmospheric medium (Ramaty and Murphy, 1987; Murphy, Dermer, and Ramaty, 1987). The cross section of pion production increases dramatically above the threshold of  $\approx 300$  MeV up to 1 GeV, then it grows gradually (see, *e.g.*, Murphy, Dermer, and Ramaty, 1987). Recall that the low-energy threshold of particles detected by high-latitude neutron monitors (NMs) is  $\approx 450$  MeV, which is specified by atmospheric absorption, but the effective energy exceeds 600–700 MeV. The minimum detected energy for medium- and low-latitude NMs is even higher and it is determined by the geomagnetic cut-off rigidity. It follows that protons producing the pion-decay emission and protons responsible for GLE belong to the same energy range. Comparison of the pion-decay emission time profile with GLE onset was earlier performed by Kurt *et al.* (2013a, 2013b and references therein).

Accelerated particles flow along field lines returning to the Sun and open field lines to produce SEPs. When high-energy protons interact with the matter, pion-decay  $\gamma$ -rays are

emitted almost instantly. Therefore, the temporal behavior of this emission can be regarded as a temporal behavior of the process of high-energy ion acceleration. Although there is no way to observe the time of accelerated high-energy protons escaping the Sun, we have a chance to estimate the time of particle release from the Sun relative to the time when pion-decay emission occurs. Indeed, hard X-ray emission (HXR) carries information as regards accelerated and precipitated electrons. Type III radio emission indicates accelerated electrons having a velocity about  $0.3c$  and moving upward along the open field lines. Thus, if pion-decay, HXR, and type III emissions occur almost simultaneously, we can assume that the possibility of acceleration and escape for protons is the same.

The observed GLE 72 was associated with the major eruptive event on 10 September 2017 that occurred in the active region (AR) 126373 near the west solar limb (S05W88) with an X8.3 importance (GOES 13). The results of neutral emission measurements during this event in a broad range of wavelengths (energy bands) have been published recently (e.g. Omodei *et al.*, 2018; Gary *et al.*, 2018; Gopalswamy *et al.*, 2018; Seaton and Darnel, 2018; Yan *et al.*, 2018; Polito *et al.*, 2018; Chertok, 2018; Warren *et al.*, 2018). The GLE 72 was observed by the worldwide NM network (<http://www.nmdb.eu>). A variety of works describing the GLE 72 properties have been published recently (e.g. Augusto *et al.*, 2019; Kurt *et al.*, 2018; Zhao, Le, and Chi, 2018; Gopalswamy *et al.*, 2018; Mishev *et al.*, 2018; Cohen and Mewaldt, 2018). For the first time since 2012, the response to these SEPs was observed in dosimetric measurements inside the *International Space Station* (Berger *et al.*, 2018). GLE 72 was also observed by the instrument orbiting the Moon (Schwadron *et al.*, 2018) and by the dosimetric experiment on the surface of Mars (Ehresmann *et al.*, 2018). This X8.2 flare and CME eruption triggered an extraordinary global extreme-ultraviolet event (Liu *et al.*, 2018).

The goals of this article are: a) based on the NM network observations of GLE 72 to determine the time interval when “the most successful” (arriving at the Earth) high-energy particles escaped from the Sun; b) to find using the available neutral emission data whether the first high-energy particles coming to Earth are accelerated in the flare itself or when a shock wave propagated in the upper part of the solar corona.

## 2. Selection of SEP and GLE data

The propagation of particles in the interplanetary magnetic field (IMF) is a complex process controlled by a variety of factors. Strauss *et al.* (2017) showed that the effects of scattering (in pitch angle) when these particles propagate from the Sun to the Earth should be taken into account in the study of GLE events, especially their temporal profiles at the beginning of the event. The angular separation of the site of the observation at the Earth and the Sun affects this propagation (Kallenrode and Wibberenz, 1990; Tylka and Lee, 2006; Gopalswamy *et al.*, 2013, 2018; Plotnikov, Rouillard, and Share, 2017). In addition, we should include magnetospheric transmissivity to correctly interpret the ground-based measurements. SEP observations up to  $\approx 700$  MeV proton energies onboard GOES satellites allow us to compare the time profile of GLE 72 obtained from the NM network data with time profiles of high-energy proton fluxes observed in the outer magnetosphere, which are very slightly shielded by the geomagnetic field.

Firstly an overview of the solar event and the SPE and GLE is presented. The derivative of the soft X-ray (SXR) flux,  $dI_{\text{SXR}}/dt$ , measured in the  $1-8 \text{ \AA}$  channel by GOES 13 indicates qualitatively the time behavior of the flare energy release, as illustrated in Figure 1a and b. High-energy proton fluxes measured with the *High Energy*

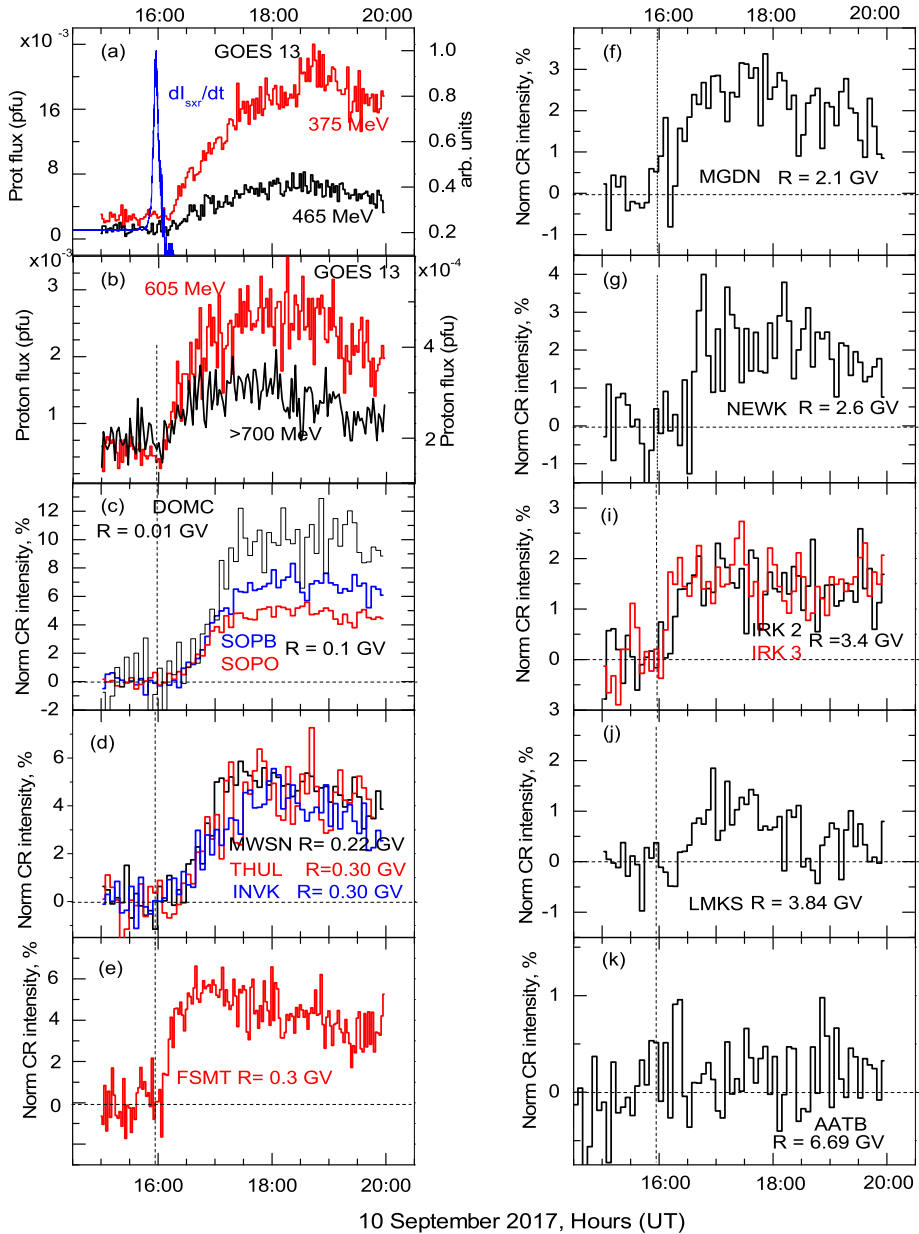


**Figure 1** Time profiles of the GLE 72 and the SEP event on 10 September 2017. GOES 13/HEPAD data and energy nominations were downloaded from <https://satdat.ngdc.noaa.gov/sem/goes/data/avg/2017/09/goes13/csv/>. P8, P9, and P10 energy ranges are 350–420, 420–510, 510–700 MeV corresponding to proton fluxes of 375 MeV, 465 MeV, 605 MeV in units of  $\text{p cm}^{-2} \text{s}^{-1} \text{sr}^{-1} \text{MeV}^{-1}$ , P11 is the integral flux of > 700 MeV in  $\text{p cm}^{-2} \text{s}^{-1} \text{sr}^{-1}$ . (a): Time profiles of P8 and P9 protons (labels on the left axis) and derivative of  $I_{sxt}$  measured by GOES 13 (blue line labels on the right axis). (b): Time profiles of P10 and P11. (c)–(g) Display the time profiles of the GLE as measured by selected NMs with various values of the cut-off rigidities,  $R_c$ .

*Proton and Alpha Detector* (HEPAD) onboard GOES 13 (located in the outer magnetosphere at  $75.4^\circ$  west longitude and  $0.045$  orbit inclination) are given in these panels (<https://satdat.ngdc.noaa.gov/sem/goes/data/avg/2017/09/goes13/csv/>). The flare onset time was observed at 15:38 UT. The main flare energy release was observed near 16:00 UT (see Figure 6 for details). Observations by the *Large Angle and Spectrometric Coronagraph* onboard the *Solar and Heliospheric Observatory* (SOHO/LASCO C2) showed the presence of CME signatures at 16:00:07 UT. Gopalswamy *et al.* (2018) studied the kinematics of the CME associated shock and the flare. According to their results the flare was accompanied by a CME with an initial speed of  $4029 \pm 163 \text{ km s}^{-1}$ , one of the highest in the SOHO era. The solar wind velocity during the time interval of 7–10 September 2017 changed considerably, from 490 up to  $810 \text{ km s}^{-1}$  (data from <https://omniweb.gsfc.nasa.gov>). The solar wind velocity was  $\approx 500 \text{ km s}^{-1}$  during the time interval of the flare energy release and beginning of the SEP event and GLE. Therefore, the base of the IMF field lines passing through the Earth was located at  $\approx 40^\circ - 45^\circ$  to the east of the flare longitude.

Time profiles of this GLE event observed by several NMs with various cut-off rigidity values are given in Figure 1c–j. The count rate of high-latitude near-sea level NMs did not exceed  $\approx 7\%$  in 2-min averages. However, the high-altitude South Pole (SOPO) NM and the Dome C (DOMC) device situated at 3233 m ([www.nmdb.eu](http://www.nmdb.eu)) recorded a higher increase. Middle- and low-latitude near-sea level NMs did not record any clear increase. However, two high-mountain middle-latitude NMs, Lomnický štít (LMKS) and Almaty (AATB), indicate a slight increase, as seen in Figure 1j and k. A small increase of the count rate of the Almaty B (AATB) NM, where the cut-off rigidity is 6.69 GV, testifies that the maximum energy of accelerated protons was not less than 6 GeV (Figure 1k). Despite the considerable angular distance between the flare location and the more probable longitude of magnetic field lines which connected to the Earth, the onsets of the SEP event and GLE were observed with a short time lag relative to the derivative of the soft X-ray (SXR) emission time (flare main energy release).

### 3. Asymptotic Directions of Selected NMs

Let us look at the anisotropy during the beginning of the event. The anisotropy is usually estimated by the comparison of count rates of northern and southern near-polar NMs. Some anisotropy effects could also be due to an angular distance of the source location and the root of IMF connecting Sun and Earth (GLE 69, Bütikofer *et al.*, 2009) or unusual angular distribution (*e.g.*, GLE 44, Cramp *et al.*, 1997). The asymptotic directions of NMs at high latitudes (not polar stations) have rather narrow cones of acceptance in the longitude extent and they collect cosmic-ray (CR) particles from regions near the equator. The ring of such stations as the *Spaceship Earth* is used for space weather studies (Bieber and Evenson, 1995). All high-latitude NMs situated near sea level have approximately the same dependence on the count rate of the energy of primary CRs. They should display almost the same increases caused by solar CRs, if the effect is an isotropic one. Thule (THUL) and Korean Jang Bogo (JBGO) NMs are looking towards the north and the south (by asymptotic directions indicated in *Spaceship Earth*). North-south anisotropy during GLE 72 is not seen (Figure 1 in the article by Kurt *et al.*, 2018). The pressure corrected cosmic-ray data from NMs were obtained from the high resolution neutron monitor database (NMDB, <http://www.nmdb.eu>). A list of the used NMs in this work with their characteristics (abbreviation, geographic coordinates, altitude and cut-off rigidity) is given in Table 1.

**Table 1** List of the NM stations, whose data has been used in this work, with their characteristics.

No	Station name	Abbr.	Lat. (°)	Long. (°)	Alt. (m)	Cut-off rigidity (GV)
1	Almaty NM, Kazakhstan	AATB	43.14°	76.60°	3340	6.69
2	Apatity NM, Russia	APTY	67.57°	33.40°	181	0.65
3	Baksan NM, Russia	BKSN	43.28°	42.69°	1700	5.60
4	Dome C Antarctica	DOMC	75.60°	123.00°	3233	< 0.1
5	Fort Smith NM, Bartol, USA	FSMT	60.02°	-111.93°	180	0.30
6	Inuvik NM, Bartol, USA	INVK	68.36°	-133.72°	21	0.30
7	Irkutsk NM, Russia	IRK2	52.47°	104.03°	2000	3.64
8	Irkutsk NM, Russia	IRK3	52.47°	104.03°	3000	3.64
9	Kerguelen NM, France	KERG	-49.35°	70.25°	33	1.14
10	Lomnický štít NM, Slovakia	LMKS	49.20°	20.22°	2634	3.84
11	Magadan NM, Russia	MGDN	60.04°	151.05°	220	2.09
12	Mawson NM, Antarctica	MWSN	-67.60°	62.88°	30	0.22
13	McMurdo NM, Bartol, USA	MCMU	-77.90°	166.60°	48	0.30
14	Nain NM, Bartol, USA	NAIN	56.55°	-61.68°	46	0.30
15	Newark NM, Bartol, USA	NEWK	39.68°	-75.75°	50	2.40
16	Oulu NM, Finland	OULU	65.05°	25.47°	15	0.80
17	Peawanuck NM, Bartol, USA	PWNK	54.98°	-85.44°	53	0.30
18	South Pole Bare NM, Bartol, USA	SOPB	-90.00°	N/A	2820	0.10
19	South Pole, Bartol, USA	SOPO	-90.00°	N/A	2820	0.10
20	Terre Adelie NM France	TERA	-66.65°	140.00°	32	0.00
21	Thule NM, Bartol, USA	THUL	76.50°	-68.70°	26	0.30
22	Tixie Bay NM, Russia	TXBY	71.36°	128.54°	sea level	0.48

For checking the longitudinal anisotropy we selected 11 stations with nominal vertical geomagnetic cut-off rigidity  $R_c < 1.4$  GV: Apatity (APTY), Fort Smith (FSMT), Inuvik (INVK), Kerguelen (KERG), Mawson (MWSN), Nain (NAIN), Oulu (OULU), Peawanuck (PWNK), Terre Adelie (TERA), Thule (THUL), and Tixie Bay (TXBY), and with standard atmospheric pressure  $> 980$  mbar. The main feature of individual NM data is their rather high statistical error value, which is  $\approx 1\%$ . Averaged over 15:00–16:00 UT of 10 September 2017 data from these NMs excluding FSMT (red line) are presented in Figure 2 together with FSMT data (black line). For the averaged variations the statistical error decreased at least by a factor of 4 in comparison with 1-min data of a typical NM. We can see that FSMT shows a rather high increase among high-latitude stations during this event. Probably a narrow beam of particles broke through to the Earth which was observed by only one NM station. Being one of the stations of *Spaceship Earth*, FSMT NM has  $< 20^\circ$  extent of asymptotic longitudes and its asymptotic latitudes are close to the equator (Figure 2 in Kuwabara *et al.*, 2006); this indicates for sure the anisotropy of the GLE 72 in the first phase of its detection.

To estimate the pitch-angle distribution beyond the magnetosphere of solar particles detected by NMs, we calculated the asymptotic directions of CR acceptance for high-latitude NMs at the onset of the GLE. These directions are defined as directions of trial particle velocities during their crossing of the magnetospheric boundary. Calculations were performed using the Tsyganenko-89 model at the onset time of the GLE event (Tsyganenko, 1989;

**Figure 2** Barometric pressure corrected count rates (1 min) from sea level NMs at positions with  $R_c < 1.14$  GV (KERG, TXBY, JBGO, THUL, OULU, FSMT, NAIN, MWSN, TERA, APTY, INVK, PWNK) are presented. The time profiles of averages of all NMs excluding FSMT are indicated with a *black line*, while the profile of FSMT is indicated with a *red line*. The *light-gray line* shows 1-min data of a typical NM. The normalization to unity was done for the interval 15:00–16:00 UT.

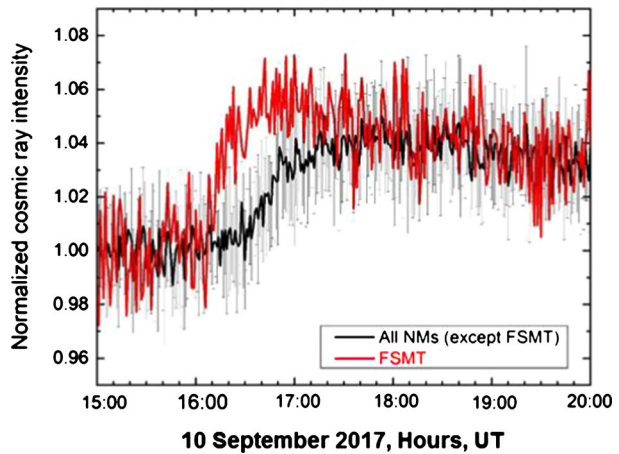
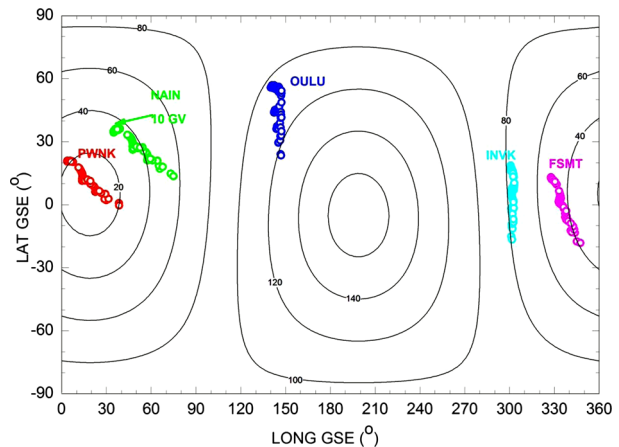


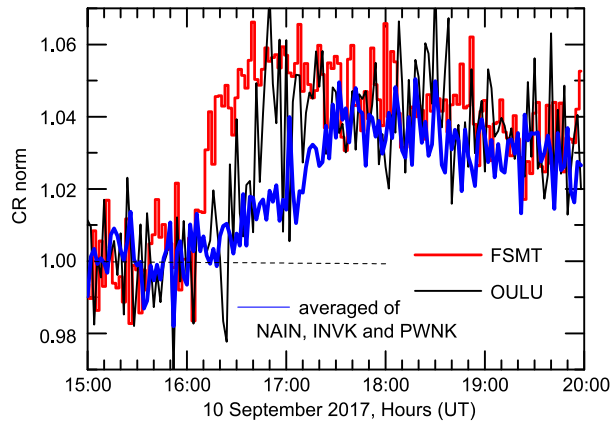
**Figure 3** The asymptotic directions of the selected NMs: INVK, FSMT, PWNK, NAIN, and OULU in the GSE coordinate system. Points with rigidities of 1–10 GV are shown (the point at lowest latitude corresponds to 1 GV). Lines with labels correspond to the pitch angle for the average direction of the IMF during the interval 16–17 UT on 10 September 2017 ( $B_x = 4.4$  nT,  $B_y = 1.5$  nT,  $B_z = 0.4$  nT in GSE).



Plainaki *et al.*, 2009). The asymptotic directions for five NM stations in the range from the cut-off rigidity of the station up to 10 GV are presented in Figure 3. Except for the FSMT station, which was the first one recording this GLE event, four neighboring sea level stations, INVK, NAIN, PWNK, and OULU, were selected to be studied. Then these asymptotic directions were compared with the IMF direction. During the interval 16–17 UT of 10 September 2017, the IMF vector had the following average components:  $B_x = 4.4$  nT,  $B_y = 1.5$  nT,  $B_z = 0.4$  nT (geocentric solar-ecliptic (GSE) system, hourly data from averaged 1-s data at <https://cdaweb.sci.gsfc.nasa.gov>). The spatial pitch-angle distribution regarding the IMF vector in combination with the asymptotic directions of selected NMs is presented in Figure 3. Assuming the access of particles at the magnetospheric boundary to be radial, the pitch angle (angle between IMF vector and radial direction) was estimated from IMF data. Plots of asymptotic directions and contours of equal pitch angles in GSE are consistent with Figure 4 of the article by Mishev *et al.* (2018).

The time profiles of the cosmic-ray intensity increase as recorded at the selected five NMs in Figure 3, and they are presented in Figure 4. We observe again that FSMT data (red line) present increasing count rates during the event in comparison with the neighboring stations NAIN, INVK, and PWNK (blue line). The onset time of OULU occurred later, with

**Figure 4** Time profiles of NMs FSMT (red line), of OULU (gray line), and of the averaged values of NAIN, INVK, and PWNK (blue line). The normalization to unity was done for the interval 15:00–16:00 UT.



a pulse-like shape profile in the count rate. The event became completely isotropic after about 18:00 UT of that day. The pitch-angle distribution and spectra of high-energy protons during GLE 72 and associated SEP event have been recently published (Mishev, Tuohino, and Usoskin, 2018; Cohen and Mewaldt, 2018).

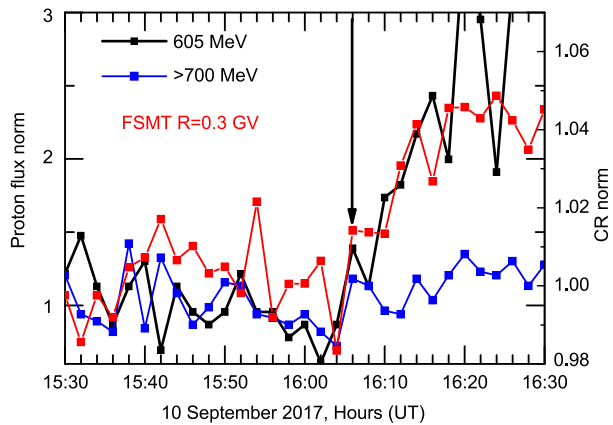
At this point it should be understood that the estimate of the pitch angle has to be taken with special caution. First, the IMF measured in the interplanetary space at the single point of SOHO/LASCO uniformly distributed throughout the space in the near Earth environment. This can be seen in comparison with the *Advanced Composition Explorer* (ACE) and *Deep Space Climate Observatory* (DSCOVR) IMF data for some periods (not shown here). During 16:00–16:10 UT the angular difference of the IMF at the two probes was  $\approx 30^\circ$ . Unfortunately, for the period of GLE 72 the data from another point in the interplanetary space with the measurements of IMF, namely on-board spacecraft *Wind*, are not available. Near the Earth the situation is also complicated by the presence of the bow shock: in the foreshock (region of interplanetary space outside the magnetosphere which is magnetically connected to the Earth's bow shock) the field may be significantly different from that in the other longitudes on the day side. Another point is that the value of the gyroradius of SEP has to be taken into consideration, since protons propagate through the regions with variable IMF (spatial structures on scales comparable with the gyroradius; differences in simultaneous ACE and DSCOVR measurements) before arriving at the magnetospheric boundary. Another issue is the rather big variation of the IMF during short time intervals (1-s data).

To investigate the SEP event and GLE onset time, we show the FSMT station count rate in the interval 15:00–16:40 UT together with the CR flux observed by GOES/HEPAD with the same time resolution (2 min) in Figure 5. The statistical significance of the increase in each curve of this figure may be insufficient, but the simultaneity of the beginning allows us to determine this time interval as  $16:07 \pm 1$  min UT. Combining the results of Figure 3 with the result deduced from Figure 5, we may conclude that the half-width (HW) of the beam at the beginning of the event does not exceed  $30^\circ$ . Taking into account that the effect is created not only (and not so much) by particles with vertical incidence on the detector, this value should be even smaller.

Since this GLE is not observed by low-latitude NMs, it can be argued that practically the whole effect of solar CRs observed at Earth is conditioned by particles in a rather limited narrow energy interval. These particles are collected from the low-latitude (near-equatorial) zone by the majority of NMs. The first ones to arrive are particles of maximum energies moving along the shortest path. The GLE 72 (and associated SEP) spectrum has a rather



**Figure 5** GOES/HEPAD proton fluxes at 605 MeV (black line) and > 700 MeV (blue line), and 2-minute cosmic ray data from the FSMT NM (red line) are given at the SPE event and GLE 72 onset time. The black arrow indicates the time of simultaneous intensity jump at 16:06–16:08 UT. The normalization to unity was done for 15:00–16:00 UT.



complicated character (Cohen and Mewaldt, 2018). Based on low-altitude NM measurements, the GLE 72 spectrum is soft in comparison with the satellite data (Figure 7). However, two high-mountain NMs show a small response too, indicating that acceleration could take place up to 6.7 GV. On the other hand, the first increase (FSMT) is not seen at high-mountain middle-latitude NMs. Thus, for calculations of the particle release time we use a proton kinetic energy  $\approx 1$  GeV ( $v \approx 0.87 c$ ).

Having determined the onset time of the SEP event and GLE as  $16:07 \pm 1$  min UT, we propose to compare this interval with the various neutral emission times. Let us discuss whether the first particles that came to Earth were accelerated during the time of the main energy release of the flare, or if the acceleration occurred at the front of the shock wave. It is possible to test models by making direct comparisons between the flare ion population evolution derived from the observations of *Fermi*/LAT (*Large Area Telescope*, Atwood *et al.*, 2009) and the SEP event and GLE onset times in the comparable energy intervals.

#### 4. Multi-Wavelength Observations of the Solar Eruptive Event and SEP and GLE Characteristics

We will clarify the scenario of the particle acceleration and release using already published data (Seaton and Darnel, 2018; Gary *et al.*, 2018; Omodei *et al.*, 2018; Yan *et al.*, 2018). There are two assumptions for explaining the origin of high-energy charged particles responsible for the GLE onset: acceleration in the solar atmosphere during the solar flare and acceleration by the CME shock wave. These assumptions are related to different scenarios, resulting in different paths of charged particles and their release time. All options should agree with the SEP event and GLE characteristics that allow us to choose the most probable one. Let us see whether we can find useful information on the release time of high-energy protons from the multi-wavelength observations related to this eruptive event. This event has a significant set of data in various ranges including X-ray and  $\gamma$ -emission spatial observations, suggesting information as regards precipitation of accelerated electrons and protons into the solar atmosphere, microwave and meter radio ranges, and extreme-ultraviolet (EUV) data describing the behavior of coronal structures.

It is assumed that particle acceleration and subsequent plasma heating are the results of magnetic reconnection (see the reviews by Fletcher *et al.*, 2011 and Zharkova *et al.*, 2011). One of the plausible scenarios is that high-energy sub-relativistic protons production begins

in the turbulent reconnecting current sheet simultaneously with or after the release of the essential energy of the flare (see for example Litvinenko and Somov, 1995; Petrosian, 2012). The time of proton acceleration and succeeding output into the interplanetary space could be determined by the culmination of these processes.

Usually the time of maximum energy release is defined on the basis of the available data at the time of X-ray flare emissions. If we are interested in the behavior of accelerated electrons, first of all we should pay attention to the Neupert effect (Neupert, 1968). This effect agrees with the time profile of SXR from the time integral of non-thermal emissions. As a result, the time behavior of the emission derivative is close to the temporal behavior of hard X-ray (HXR) emission generated by accelerated electrons. This effect is observed in many flares and can be considered with a high degree of accuracy to be a “proxy” of the time behavior of flare energy release during the flare impulsive phase (Dennis and Zarro, 1993; Veronig *et al.*, 2002; Dennis *et al.*, 2003). This effect can only take place when accelerated electrons provide energy to the SXR emitted volume after the gas dynamic heating of the solar atmosphere resulting in SXR emission. This method can be used to study limb events and/or partly occulted events.

In this work, we analyze the acceleration processes during the flare using the time profile of the SXR emission derivative, the time profile of 50–100 keV and 100–300 keV HXR emission, and the time profile of the 0.8–7 MeV  $\gamma$ -emission using observations by the *Reuven Ramaty High Energy Solar Spectroscopic Imager* (RHESSI). They are presented in Figure 6. The 50–300 keV count rate is caused by bremsstrahlung. The count rate in the 0.8–7 MeV energy interval contains both HXR bremsstrahlung and emission of  $\gamma$ -lines. There are two main peaks at the energy range up to 300 keV. The onset in the first peak was at about 15:53 UT. The onset of the second one was at 15:56:30 UT. The second peak consisted of three subpeaks, which began at 15:56:30, 15:57:45, and 15:59:30 UT. The SXR derivative tracks the above-mentioned HXR pulses. The count rate of the 0.8–7 MeV energy band increased gradually and then abruptly jumped also at 15:57:45 UT and at 15:59:30 UT. We can see that all the time profiles have maxima at this time. Gary *et al.* (2018) also indicated the maximum time at about 15:58 UT according to microwave observations carried out with the *Expanded Owens Valley Solar Array* (EOVSA).

The comparison of HXR and SXR derivative time profiles with the time behavior of high-energy pion-decay emission  $E_\gamma > 100$  MeV observed by *Fermi*/LAT (Omodei *et al.*, 2018) demonstrated a close relationship between the time behavior of the impulsive phase energy release and the appearance of high-energy protons. Omodei *et al.* (2018) results, taken from Table 2, are shown in Figure 6. It is seen that *Fermi*/LAT detected the onset of high-energy emission created by pion-decay at 15:56:55–15:57:55 UT. The pion-decay maximum was observed between 15:59:25–16:01:25 UT. From this panel it is possible to note how the proton index changed during the impulsive phase of the flare. The proton index derived from the photon spectra is the hardest in time interval 15:58:54–16:01:54 UT, with a value 3.2–3.5 (Figure 2 and Table 1 in Omodei *et al.*, 2018). Thus the most intense pion production time interval is in full agreement with the period of the more intensive flare energy release between 15:58–16:02 UT.

We can assume the main maximum time as the onset of charged particles acceleration and their escape into interplanetary space. However, this flare was associated with a CME. That is why we have to test the shock wave role in the acceleration of the charged particles (for example Reames, 2013; Ryan, Lockwood, and Debrunner, 2000; Ryan, 2000). Usually, a flux rope eruption is followed by mass inflow, the formation of a current sheet and a cusp structure, which were simultaneously observed during this flare in EUV and X-rays. We show the comparison of different observational results in Figure 6c). Yan *et al.* (2018)

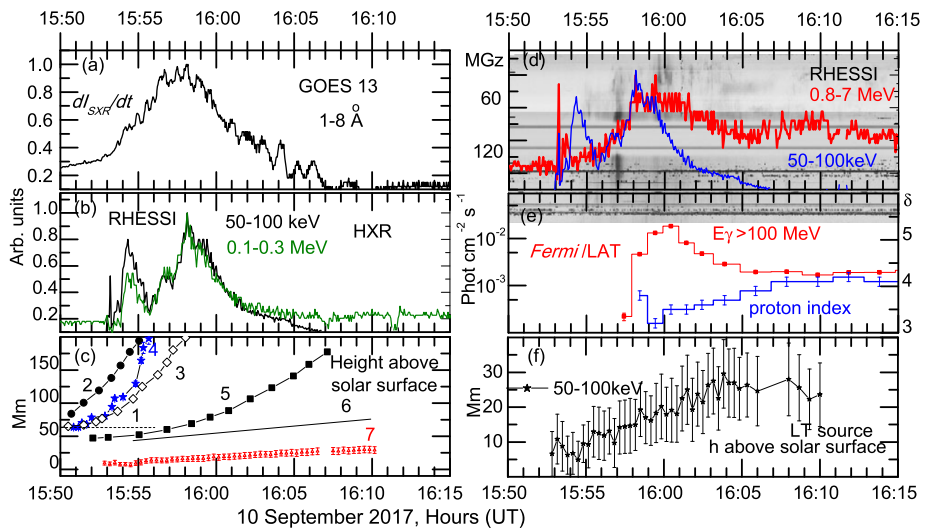


**Figure 6** Left panels: (a) time variation of  $dI_{SXR}/dt$  (GOES13, 1–8 Å), (b) HXR-50–100 keV (black), 0.1–0.3 MeV (olive) (RHESSI data), (c) composite height-time dependencies of the motion of the different structures obtained from EUV and X-ray images. Lines 1, 2, 3 inferred from EUV image observations and taken from trajectories of Figure 2d of Yan *et al.* (2018). The slow rise of the flux rope is presented with the dotted line 1. The black lines 2, 3, with circles and diamonds outline the acceleration stage of the flux rope top and the bottom of the flux rope, respectively. The blue line 4 with asterisks indicates the trajectory of the flux rope measured with SUVI and it is taken from Figure 2 of Seaton and Darnel (2018). Curve 5 with black squares corresponds to the cusp-shaped structure. The black line 6 is the motion of the post-flare loops, curve 5 and line 6 are taken from the same publication as 1–3 lines. Line 7 is the 25–50 keV HXR LT source motion. Right panels: (d) time profiles of 50–100 keV HXR and 0.8–7 MeV  $\gamma$  rays (RHESSI) combined in time with the radio emission measured by the Sagamore Hill Radio Observatory, (e) photon flux  $E_\gamma > 100$  MeV (left scale) and proton spectral index  $\delta$  (Fermi/LAT data from Table 1 of Omodei *et al.*, 2018), (f) time-height dependence of the LT source with energies in the range 50–100 keV (black stars with errors).

determined the trajectories of dynamic structures using the *Atmospheric Imaging Assembly* data (AIA: Lemen *et al.*, 2012) onboard the Solar Dynamics Observatory (SDO). The flux rope rising measurements as a function of height were made with the *Solar Ultraviolet Imager* (SUVI) on GOES 16 spacecraft (Seaton and Darnel, 2018). Besides we estimate the time-height dependence of the HXR source of 25–50 keV obtained from the X-ray images. The X-ray images were reconstructed by using RHESSI data and the standard software for their processing (Hurford *et al.*, 2002). The HXR images at 25–50 keV and 50–100 keV energy bands were reconstructed with a 20-s time bin using the CLEAN algorithm for 6F and 8F detectors. The position of the loop top (LT) source was defined as the centroid position of the image intensity distribution. This allows us to calculate the distance between the LT source and the solar limb.

One can see the flux rope rising before the appearance of the HXR LT source. This fact indicates the onset of the reconnection process approximately at 15:53 UT and agrees with the first HXR peak seen in the 50–300 keV energy band. The LASCO CME catalogue estimated the CME onset time at about 15:52 UT. Thus, we can explain the first HXR peak by the model synchronizing the CME dynamics and the reconnection process in the current sheet beneath the CME (Temmer *et al.*, 2008). So the CME shock wave appeared in the AR before the next peak, which was related not only with HXR emission of accelerated

electrons but with pion-decay  $\gamma$ -emission. Generally speaking, it should be safe to assume that a CME shock wave occurred before the appearance of the high-energy protons in the solar atmosphere. If intensive acceleration of particles by the CME shock wave is underway, then this implies an increase of the observed source height and size because the source should move away from the solar surface. Omodei *et al.* (2018) localized the source of pion-decay emission with  $E_\gamma > 100$  MeV for three different time “windows” of the event (see Figure 3 of the cited article). One can see that the most probable location of the source between 15:56–16:06 UT coincided with the active region and the cusp-shaped structure. The increase in size and the motion of the source were detected 3 h later during the second time interval.

The other evidence of desynchronization of the CME with the SEP event and GLE beginning is the onset times and frequencies of type II bursts. According to information from the NOAA event list, a type II burst was detected at 16:08 UT in the 25–43 MHz frequencies. These frequencies mean that the emission was generated at more than one solar radius distance from the solar limb.

However, we see the steady upward motion of a 50–100 keV LT source after 15:57 UT. This could be related with the enhancement of the reconnection rate, which results in a very efficient particle acceleration (Kopp and Pneuman, 1976; Kopp and Poletto, 1984; Poletto and Kopp, 1986; Sui and Holman, 2003; Li and Gan, 2005). The formation of a current sheet and a cusp structure continued after the CME related with the flux rope eruption. The average velocity of the post-flare loop rising was  $35.4 \pm 3.0$  km s<sup>-1</sup>. It was derived from the flux rope movement by SUVI source motion (Figure 6c, line 4). The average velocity of the HXR LT source rise was about 20 km s<sup>-1</sup>.

Models by Litvinenko and Somov (1995) and Petrosian (2012) assume that sub-relativistic proton production begins in the turbulent reconnecting current sheet. We emphasize that pion-decay onset and maximum was observed by *Fermi*/LAT at 16:56:55–16:57:55 UT and at 15:58:54–16:00:54 UT, respectively, when the current sheet feature became evidently visible on series of AIA 193 Å images (see Warren *et al.*, 2018). Moreover, these authors have found Fe XXIV (192.04 Å) line broadening in the current sheet. The observed line width results from the combination of thermal broadening, instrumental broadening, and non-thermal turbulent motions of the plasma. Warren *et al.* (2018) concluded that strong non-thermal turbulent velocity broadening with approximately 70–150 km s<sup>-1</sup> existed in the current sheet. This broadening increased with height above the limb and then gradually declined.

The facts presented indicate that pion-decay emission with  $E_\gamma > 100$  MeV was generated during the maximum of the flare impulsive phase. At the same time the CME onset and the type II burst detection time poorly agree with the *Fermi*/LAT data. Moreover, Figure 6d shows the time resemblance between 15:59:30–16:01:30 UT of type III bursts at 25–43 MHz frequencies, of the second maximum of the HXR flux, of 0.8–7 MeV, and of pion-decay emission maximum. A type III burst indicates escaping of the accelerated electrons and assumes a good possibility for the escaping of other particles.

Let us come back to GLE 72 and SPE onset time intervals. We derive the GLE and SEP event onset time at  $16:07 \pm 1$  min UT. We explore the assumption that protons were accelerated during the flare. Some of them immediately went down and created pion-decay emission, the others ran away along the open magnetic field lines like the electrons, which created the type III at  $16:00:30 \pm 30$  s UT. Pion-decay maximum was also observed at 15:58:54–16:00:54 UT. Let us assume that this interval is the time of particle release from the Sun. Considering that the most plausible energy for particles responsible for the GLE onset equal to 5 GeV or 1 GeV ( $v = 0.98 c$  or  $0.87 c$ ), we calculate the likeliest particle

path length based on the difference of the observed onset times of GLE and SPE and the proposed release time. We get a path length equal to  $1.6 \pm 0.1$  AU.

Efficient energy of SEPs (channel P10 of HEPAD in GOES 13) is 605 MeV ( $v = 0.79 c$ ). So, we get for the SEPs a path length equal to  $1.4 \pm 0.4$  AU. We should keep in mind that the half-width (HW) of the beam at the beginning of the event does not exceed  $30^\circ$ . The injection profile (simply a delta function) is not the only controlling factor of the pulse shape of GLEs; interplanetary transport conditions can also have a strong influence. Of course, the particles that stream along the magnetic field, *i.e.* that have pitch angle  $\alpha = 0^\circ$ , reach the Earth first, and their profile shows a very quick rise (*i.e.* a short rise time). Particles mostly gyrating perpendicular to the field ( $\alpha = 90^\circ$ ), take longer to reach Earth but also have a longer rise time. Even at the beginning of the event particles are experiencing some pitch-angle scattering (Strauss *et al.*, 2017). This leads to some increase of the path length. Bearing in mind the previous discussion and assuming a Parker spiral nominal length of 1.2 AU and a 10–15% error due to the variability of the observed solar wind velocities, we conclude that this path length is  $\approx 1.5 \pm 0.3$  AU in accordance with the IMF lines length in the period under study.

## 5. Concluding Remarks

In this work a study of the GLE 72 event on 10 September 2017 and its relationship with the neutral emissions observed during the eruptive event SOL2017-09-10 (X8.9 solar flare), which occurred at the western limb of the Sun, is performed. We carry out a detailed analysis of the various flare emissions together with the GLE properties in order to better understand the connection between the accelerating agents of the proton population responsible for the pion-decay emission detected with *Fermi*/LAT and the solar energetic particles measured at 1 AU.

From this study the following conclusions are obtained:

1. According to the NM measurements, the amplitude of this GLE associated with the flare, was relatively small, about 8–11% (2-min averages), even at high-altitude polar NM SOPO and detector DOMC. A totally isotropic maximum of the GLE was observed at about 18:00 UT. This event is  $5-6 \sigma$  smaller than the average value in the scatter plot of maximum GLE increase *versus* maximum flux of the SPE event at energies  $E_p > 100$  MeV (P100) observed at the *Interplanetary Monitoring Platform* (IMP) and GOES satellite data (Figure 7). Contrary to NM observations, proton flux with energies

**Figure 7** Scatter plot of maximum increase of GLEs *versus* maximum flux of protons with energies  $E_p > 100$  MeV for various GLEs. The *red star* corresponds to the GLE on 10 September 2017. The *blue diamond* in the *upper right corner* corresponds to the GLE on 20 January 2005 (from Kurt *et al.*, 2018).

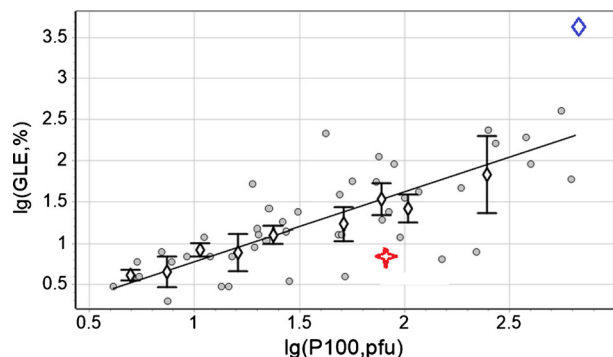
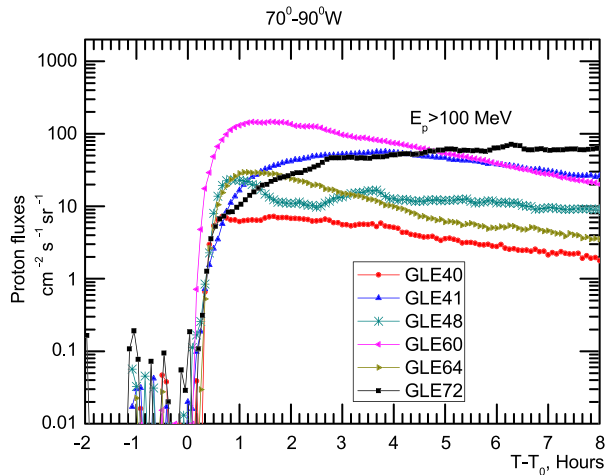


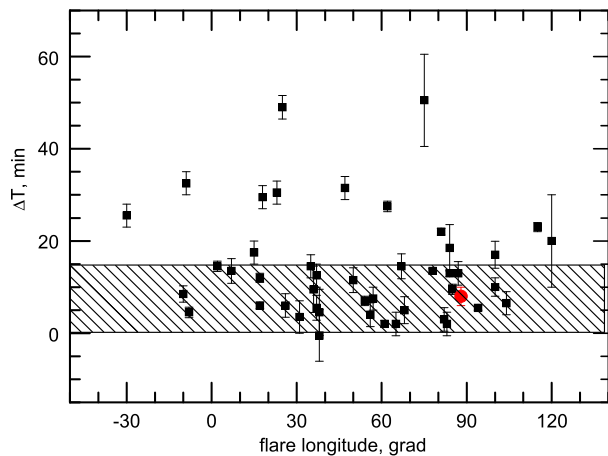
**Figure 8** Time profiles of SEP events with proton energies  $E_p > 100$  MeV associated with GLEs connected with parent flares located between  $70^\circ - 90^\circ$  W.



$E_p > 100$  MeV was  $\sim 70$  pfu. It was the second largest flux in the  $\approx 70$  pfu. It is the second largest flux in the  $70^\circ - 90^\circ$  W longitude interval of the parent flare (see Figure 8).

2. No north-south anisotropy is found in the event.
3. The asymptotic directions of CRs for five near-sea-level NMs at high latitudes (geomagnetic cut-off rigidity  $R_c < 1.4$  GV) are calculated. A high level of the west-east anisotropy is observed at the event beginning (FSMT with respect to other high-latitude NMs).
4. From the available electromagnetic emission observations, the following facts are deduced:
  - The time interval of the highest maximum of HXR emission at 15:58–16:01 UT is the flare energy release maximum.
  - The onset time of  $E_\gamma > 100$  MeV pion-decay emission (high-energy proton acceleration) at 15:56:55–15:57:55 UT and maximum between 15:58:54–16:00:54 UT observed with *Fermi*/LAT (Omodei *et al.*, 2018) is in accordance with the main flare energy release time. This time interval of the impulsive  $> 100$  MeV  $\gamma$ -emission is relevant to the time of the turbulent current sheet creation.
  - Multiple type III bursts indicate that the accelerated electrons are moving upward along the open field lines around the time of the  $> 100$  MeV pion-decay emission maximum. This time interval is assumed to be the release time of high-energy protons.
5. The GLE and SEP event onset time is determined to be at 16:06–16:08 UT. Using the release time of particles between 16:00–6:01 UT we calculate a path length for 0.7–5 GeV protons equal to  $1.5 \pm 0.3$  AU, which is in accordance with the length of IMF lines derived from the observed solar wind velocities.
6. We show that a pion-decay emission burst with  $E_\gamma > 100$  MeV appeared during the peak time of the flare impulsive phase. Furthermore the last smooth increase of this emission and count rate in the 0.8–7 MeV band (RHESSI) began at about 16:06–16:07 UT (see Figure 6), revealing a new episode of acceleration, which agrees almost exactly with the onset of the type II. Thus, this result can be consistent with the inference of Share *et al.* (2018) that protons accelerated in the process of the flare contribute to the seed population that is further accelerated by the shock and gets into the field lines

**Figure 9** Lag of GLE onset time relative to the time of flare energy release *versus* the parent flare location. The red circle corresponds to GLE 72. The sparse area shows the delay time interval 0–15 min (from Kurt *et al.*, 2013a).



returning to the Sun to produce the late-phase of  $> 100$  MeV  $\gamma$ -ray emission. These additionally accelerated particles also ran away along the open magnetic field lines and made some contribution to the total flux of particles arriving at 1 AU. Figure 8 shows the time profiles of protons  $> 100$  MeV for GLEs, associated with flares located between  $70^\circ$ – $90^\circ$  W, giving us a hint to such an opportunity for the considered SEP event.

In conclusion, the scatter plot of the time difference between each GLE onset (derived from the NM network) and the time of the maximum of the energy release *versus* the parent flare longitude, presented in Figure 9, shows that the time lag of the last GLE 72 lies in the band of the most probable values. Moreover, the pion-decay  $\gamma$ -emission observations with a good temporal resolution during the flare impulsive phase are available only in a few GLE events including the eruptive event SOL2017-09-10. It should be noted that, even in this event, we can determine the exact release time with 3–4 min accuracy, which is somewhere between the pion-decay onset and its maximum.

**Acknowledgements** The authors wish to acknowledge the PIs of all neutron monitors (<http://www.nmdb.eu>), whose data are used in this paper, and GOES data providers. N. Ness of Bartol Institute and CDAWeb are acknowledged for data providing. KK wishes to acknowledge support by the project CREAT (reg. CZ.02.1.01/0.0/0.0/15/003/0000481) call number 02 15 003 of the Operational Program Research, Development and Education. Thanks are due to the anonymous referee for useful comments and suggestions, improving this article. LKK thanks the budgetary funding of the Basic Research program II.16.

**Conflict of Interests** The authors declare that there are no conflicts of interest.

**Publisher's Note** Springer Nature remains neutral with regard to jurisdictional claims in published maps and institutional affiliations.

## References

- Atwood, W.B., Abdo, A.A., Ackermann, M., Althouse, W., Anderson, B., Axelsson, M., Baldini, L., Ballet, J., Band, D.L., Barbiellini, G., *et al.*: 2009, The large area telescope on the Fermi gamma-ray space telescope mission. *Astrophys. J.* **697**, 1071. [DOI](#).
- Augusto, C.R.A., Navia, C.E., de Oliveira, M.N., Nepomuceno, A.A., Fauth, A.C., Kopenkin, V., Sinzi, T.: 2019, Relativistic proton levels from region AR2673 (GLE #72) and the heliospheric current sheet as a Sun–Earth magnetic connection. *Publ. Astron. Soc. Pac.* **131**, 024401. [DOI](#).

- Belov, A., Eroshenko, E., Kryakunova, O., Kurt, V., Yanke, V.: 2010, Ground level enhancements of solar cosmic rays during the last three solar cycles. *Geomagn. Aeron.* **50**, 21. DOI.
- Berger, T., Matthiä, D., Burmeister, S., Rios, R., Lee, K., Semones, E., Hassler, D.H., Stoffle, N., Zeitlin, C.: 2018, The solar particle event on 10 September 2017 as observed on-board the International Space Station (ISS). *Space Weather*. DOI.
- Bieber, J.W., Evenson, P.: 1995, Spaceship Earth – An optimized network of neutron monitors. In: *Proc. 24th ICRC* **4**, 1316.
- Bütikofer, R., Flückiger, E.O., for the NMDB team: 2009, Near real-time determination of ionization and radiation dose rates induced by cosmic rays in the Earth's atmosphere – a NMDB application. In: *Proc. 31st ICRC* (in CD), icrc1137.
- Bütikofer, R., Flückiger, E.O., Desorgher, L., Moser, M.R., Pirard, B.: 2009, The solar cosmic ray ground-level enhancements on 20 January 2005 and 13 December 2006. *Adv. Space Res.* **43**, 499. DOI.
- Chertok, I.: 2018, Diagnostic analysis of the solar proton flares of September 2017 by their radio bursts. *Geomagn. Aeron.* **58**, 457. DOI.
- Cohen, C.M.S., Mewaldt, R.A.: 2018, The ground-level enhancement event of September 2017 and other large solar energetic particle events of Cycle 24. *Space Weather* **16**, 10. DOI.
- Copeland, K., Matthiä, D., Meier, M.: 2018, Solar cosmic ray dose rate assessments during GLE 72 using MIRA and PANDOCA. *Space Weather* **16**, 969. DOI.
- Cramp, J.L., Duldig, M.L., Flückiger, E.O., Humble, J.E., Shea, M.A., Smart, D.F.: 1997, The October 22, 1989, solar cosmic ray enhancement: An analysis of the anisotropy and spectral characteristics. *J. Geophys. Res.* **102**, 24237.
- Dennis, B.R., Zarro, D.M.: 1993, The Neupert effect – What can it tell us about the impulsive and gradual phases of solar flares? *Solar Phys.* **146**, 177. DOI.
- Dennis, B., Veronig, A., Schwartz, R.A., Sui, L., Tolbert, A.K., Zarro, D.M. (RHESSI Team): 2003, The Neupert effect and new RHESSI measures of the total energy in electrons accelerated in solar flares. *Adv. Space Res.* **32**, 2459. DOI.
- Duldig, M.L., Watts, D.J.: 2001, The new international GLE database. In: *Proc. ICRC 2001* **8**, 3409.
- Ehresmann, B., Hassler, D.M., Zeitlin, C., Guo, J., Wimmer-Schweingruber, R.F., Matthiä, D., Lohf, H., Burmeister, S., Rafkin, S.C.R., Berger, T., Reitz, G.: 2018, Energetic particle radiation environment observed by RAD on the surface of Mars during the September 2017 event. *Geophys. Res. Lett.* **45**, 5305. DOI.
- Fletcher, L., Dennis, B.R., Hudson, H.S., Krucker, S., Phillips, K., Veronig, A., Battaglia, M., Bone, L., Caspi, A., Chen, Q., Gallagher, P., Grigis, P.T., Ji, H., Liu, W., Milligan, R.O., Temmer, M.: 2011, An observational overview of solar flares. *Space Sci. Rev.* **159**, 19. DOI.
- Forbush, S.: 1946, Three unusual cosmic-ray increases possibly due to charged particles from the Sun. *Phys. Rev.* **70**, 771. DOI.
- Gary, D.E., Chen, B., Dennis, B.R., Fleishman, G.D., Hurford, G.J., Krucker, S., McTiernan, J.M., Nita, G.M., Shih, A.Y., White, S.M., Yu, S.: 2018, Microwave and hard X-ray observations of the 2017 September Solar limb flare. *Astrophys. J.* **863**, 83. DOI.
- Gopalswamy, N., Xie, H., Mäkelä, P., Yashiro, S., Akiyama, S., Uddin, W., Srivastava, A.K., Joshi, N.C., Chandra, R., Manoharan, P.K., Mahalakshmi, K., Dwivedi, V.C., Jain, R., Awasthi, A.K., Nitta, N.V., Aschwanden, M.J., Choudhary, D.P.: 2013, Height of shock formation in the solar corona inferred from observations of type II radio bursts and coronal mass ejections. *Adv. Space Res.* **51**, 1981. DOI.
- Gopalswamy, N., Mäkelä, P., Akiyama, S., Yashiro, S., Xie, H., Thakur, N.: 2018, Extreme kinematics of the 2017 September 10 solar eruption and the spectral characteristics of the associated energetic particles. *Astrophys. J. Lett.* **863**, L39. DOI.
- Hurford, G.J., Schmahl, E.J., Schwartz, R.A., Conway, A.J., Aschwanden, M.J., Csillaghy, A., Dennis, B.R., Johns-Krull, C., Krucker, S., Lin, R.P., McTiernan, J., Metcalf, T.L., Sato, J., Smith, D.M.: 2002, The RHESSI imaging concept. *Solar Phys.* **210**, 61. DOI.
- Kallenrode, M.-B., Wibberenz, G.: 1990, Influence of interplanetary propagation on particle onsets. In: *Proc. 21st ICRC* **5**, 229.
- Kopp, R.A., Pneuman, G.W.: 1976, Magnetic reconnection in the corona and the loop prominence phenomenon. *Solar Phys.* **50**, 85. DOI.
- Kopp, R.A., Poletto, G.: 1984, Extension of the reconnection theory of two-ribbon solar flares. *Solar Phys.* **93**, 351. DOI.
- Kurt, V., Yushkov, B., Belov, A., Chertok, I., Grechnev, V.: 2013a, Determination of acceleration time of protons responsible for the GLE onset. *J. Phys. Conf. Ser.* **409**, 012151. DOI.
- Kurt, V.G., Kudela, K., Yushkov, B.Y., Galkin, V.I.: 2013b, On the onset time of several SPE/GLE events: indications from high-energy gamma-ray and neutron measurements by CORONAS-F. *Adv. Astron.* **2013**, 690921. DOI.



- Kurt, V., Belov, A., Kudela, K., Yushkov, B.: 2018, Some characteristics of the GLE on 10 September 2017. *Contrib. Astron. Obs. Skaln. Pleso* **48**, 329.
- Kuwabara, K., Bieber, J., Clem, J., Evenson, P., Pyle, R., Munakata, K., Yasue, S., Kato, C., Akahane, S., Koyama, M., Fujii, F., Duldig, M.L., Humble, J.E., Silva, M.R., Trivedi, N.B., Gonzalez, W.D., Schuch, N.J.: 2006, Real-time cosmic ray monitoring system for space weather. *Space Weather* **4**, S08001. DOI.
- Lemen, J.R., Title, A.M., Akin, D.J., Boerner, P.F., Chou, C., Drake, J.F., Duncan, D.W., Edwards, Ch.G., Friedlaender, F.M., Heyman, G.F., Hurlburt, N.E., Katz, N.L., Kushner, G.D., Levay, M., Lindgren, R.W., Mathur, D.P., McFeaters, E.L., Mitchell, S., Rehse, R.A., Schrijver, C.J., Springer, L.A., Stern, R.A., Tarbell, T.D., Wuelser, J.-P., Wolfson, C.J., Yanari, C., Bookbinder, J.A., Cheimets, P.N., Caldwell, D., Deluca, E.E., Gates, R., Golub, L., Park, S., Podgorski, W.A., Bush, R.I., Scherrer, P.H., Gummis, M.A., Smith, P., Auker, G., Jerram, P., Pool, P., Soufli, R., Windt, D.L., Beardsley, S., Clapp, M., Lang, J., Waltham, N.: 2012, The Atmospheric Imaging Assembly (AIA) on the Solar Dynamics Observatory (SDO). *Solar Phys.* **275**, 17. DOI.
- Li, Y.-P., Gan, W.-Q.: 2005, A scenario of the X4.8 flare of 2002 July 23 based on RHESSI and TRACE observations. *Chin. Astron. Astrophys.* **29**, 61. DOI.
- Litvinenko, Yu., Somov, B.: 1995, Relativistic acceleration of protons in reconnecting current sheets of solar flares. *Solar Phys.* **158**, 317. DOI.
- Liu, W., Jin, M., Downs, C., Ofman, L., Cheung, M.C.M., Nitta, N.V.: 2018, A truly global EUV wave from the SOL2017-09-10 X8.2 solar flare-CME eruption. *Astrophys. J. Lett.* **864**, L24. DOI.
- Mavromichalaki, H., Papaioannou, A., Plainaki, C., Sarlanis, C., Souvatzoglou, G., Gerontidou, M., Papailiou, M., Eroshenko, E., Belov, A., Yanke, V., Flückiger, E.O., Büttikofer, R., Parisi, M., Storini, M., Klein, K.-L., Fuller, N., Steigies, C.T., Rother, O.M., Heber, B., Wimmer-Schweingruber, R.F., Kudela, K., Strharsky, I., Langer, R., Usoskin, I., Ibragimov, A., Chilingaryan, A., Hovsepian, G., Reymers, A., Yeghikyan, A., Kryakunova, O., Dryn, E., Nikolayevskiy, N., Dorman, L., Pustil'nik, L.: 2011, Applications and usage of the real-time neutron monitor database. *Adv. Space Res.* **47**, 2210. DOI.
- Mavromichalaki, H., Gerontidou, M., Paschalis, P., Paouris, E., Tezari, A., Sgouropoulos, C., Crosby, N., Dierckxsens, M.: 2018, Real-time detection of the ground level enhancement on 10 September 2017 by A.Ne.Mo.S.: System report. *Space Weather* **16**, 1797. DOI.
- Miroshnichenko, L.I.: 2015, *Solar Cosmic Rays: Fundamentals and Applications*, *Astrophys. and Space Sci. Lib.* **405**, Springer, Berlin.
- Mishev, A., Poluianov, S., Usoskin, I.: 2017, Assessment of spectral and angular characteristics of sub-GLE events using the global neutron monitor network. *J. Space Weather Space Clim.* **7**, A28. DOI.
- Mishev, A.L., Usoskin, I.G.: 2018, Assessment of the radiation environment at commercial jet-flight altitudes during GLE 72 on September 10, 2017 using neutron monitor data. *Space Weather* **16**, 1921. DOI.
- Mishev, A., Tuohino, S., Usoskin, I.: 2018, Neutron monitor count rate increase as a proxy for dose rate assessment at aviation altitudes during GLEs. *J. Space Weather Space Clim.* **8**, A46. DOI.
- Mishev, A., Usoskin, I., Raukunen, O., Paasilta, M., Valtonen, E., Kocharov, L., Vainio, R.: 2018, First analysis of Ground-Level Enhancement (GLE) 72 on September 2017: Spectral and anisotropy characteristics. *Solar Phys.* **293**, 136. DOI.
- Moraal, H., McCracken, K.: 2012, The time structure of ground level enhancements in Solar Cycle 23. *Space Sci. Rev.* **171**, 85. DOI.
- Murphy, R., Dermer, C., Ramaty, R.: 1987, High-energy processes in solar flares. *Astron. Astrophys. Suppl. Ser.* **63**, 721. DOI.
- Neupert, W.: 1968, Comparison of solar X-ray line emission with microwave emission during flares. *Astrophys. J. Lett.* **153**, L59. DOI.
- Omodei, N., Pesce-Rollins, M., Longo, F., Allafort, A., Krucker, S.: 2018, Fermi-LAT observations of the 2017 September 10th solar flare. *Astrophys. J. Lett.* **865**, L7. DOI.
- Petrosian, V.: 2012, Stochastic acceleration by turbulence. *Space Sci. Rev.* **173**, 535. DOI.
- Plainaki, C., Mavromichalaki, H., Belov, A., Eroshenko, E., Yanke, V.: 2009, Neutron monitor asymptotic directions of viewing during the event of 13 December 2006. *Adv. Space Res.* **43**, 518. DOI.
- Plotnikov, I., Rouillard, A., Share, G.: 2017, The magnetic connectivity of coronal shocks from behind-the-limb flares to the visible solar surface during gamma-ray events. *Astron. Astrophys.* **608**, A43. DOI.
- Poletto, G., Kopp, R.A.: 1986, Macroscopic electric fields during two-ribbon flares. In "The lower atmosphere of solar flares". In: Neidig, D. (ed.) *Proc. Solar Maximum Mission Symp.*, 453.
- Polito, V., Dudík, J., Kašparová, J., Džifčáková, E., Reeves, K.K., Testa, P., Chen, B.: 2018, Broad non-Gaussian Fe XXIV line profiles in the impulsive phase of the 2017 September 10 X8.3 class flare observed by Hinode/EIS. *Astrophys. J.* **864**, 63. DOI.
- Poluianov, S., Usoskin, I., Mishev, A., Shea, M., Smart, D.F.: 2017, GLE and sub-GLE redefinition in the light of high-altitude polar neutron monitors. *Solar Phys.* **292**, 176. DOI.
- Ramaty, R., Murphy, R.: 1987, Nuclear processes and accelerated particles in solar flares. *Space Sci. Rev.* **45**, 213. DOI.

- Reames, D.: 2013, The two sources of solar energetic particles. *Space Sci. Rev.* **175**, 53. DOI.
- Reames, D.V.: 2009a, Solar release time of energetic particles in ground-level events. *Astrophys. J.* **693**, 812. DOI.
- Reames, D.V.: 2009b, Solar energetic-particle release times in historical ground-level events. *Astrophys. J.* **706**, 844. DOI.
- Ryan, J.: 2000, Long-duration solar gamma-ray flares. *Space Sci. Rev.* **93**, 581. DOI.
- Ryan, J., Lockwood, J., Debrunner, H.: 2000, Solar energetic particles. *Space Sci. Rev.* **93**, 35. DOI.
- Schwadron, N.A., Rahmanifard, F., Wilson, J., Jordan, A.P., Spence, H.E., Joyce, C.J., Blake, J.B., Case, A.W., de Wet, W., Farrell, W.M., Kasper, J.C., Looper, M.D., Lugaz, N., Mays, L., Mazur, J.E., Niehof, J., Petro, N., Smith, C.W., Townsend, L.W., Winslow, R., Zeitlin, C.: 2018, Update on the worsening particle radiation environment observed by CReTER and 802 implications for future human deep-space exploration. *Space Weather* **16**, 289. DOI.
- Seaton, D., Darnel, J.M.: 2018, Observations of an eruptive solar flare in the extended EUV solar corona. *Astrophys. J. Lett.* **852**, L9. DOI.
- Share, G., Murphy, R., Tolbert, A.K., Dennis, B.R., White, S.M., Schwartz, R.A., Tylka, A.J.: 2018, Characteristics of sustained > 100 MeV gamma-ray emission associated with solar flares. *Astrophys. J.* **869**, 182. DOI.
- Shea, M.A., Smart, D.F.: 1990, A summary of major solar proton events. *Solar Phys.* **127**, 297. DOI.
- Shea, M.A., Smart, D.F., Pyle, K.R., Duldig, M.L., Humble, J.E.: 2001, Update on the GLE database; Solar Cycle 19. In: *Proc. ICRC 2001*, 3405.
- Souvatzoglou, G., Papaioannou, A., Mavromichalaki, H., Dimitroulakos, J., Sarlanis, C.: 2014, Optimizing the real-time ground level enhancement alert system based on neutron monitor measurements: Introducing GLE alert plus. *Space Weather* **12**, 633. DOI.
- Strauss, R.D., Ogunjobi, O., Moraal, H., McCracken, G., Caballero-Lopez, R.A.: 2017, On the pulse shape of ground-level enhancements. *Solar Phys.* **292**, 51. DOI.
- Sui, L., Holman, D.: 2003, Evidence for the formation of a large-scale current sheet in a solar flare. *Astrophys. J.* **596**, L251. DOI.
- Temmer, M., Veronig, A., Vršnak, B., Rybák, J., Gömöry, P., Stoiser, S., Maričić, D.: 2008, Acceleration in fast halo CMEs and synchronized flare HXR bursts. *Astrophys. J. Lett.* **673**, L95. DOI.
- Tsyganenko, N.A.: 1989, Magnetospheric magnetic field model with a warped tail current sheet. *Planet. Space Sci.* **37**, 5. DOI.
- Tylka, A., Lee, M.: 2006, A model for spectral and compositional variability at high energies in large, gradual solar particle events. *Astrophys. J.* **646**, 1319. DOI.
- Veronig, A., Vršnak, B., Dennis, B.R., Temmer, M., Hanslmeier, A., Magdalenic, J.: 2002, Investigation of the Neupert effect in solar flares. I. Statistical properties and the evaporation model. *Astron. Astrophys.* **392**, 699. DOI.
- Warren, H.P., Brooks, D.H., Ugarte-Urra, I., Reep, J.W., Crump, N.A., Doschek, G.A.: 2018, Spectroscopic observations of current sheet formation and evolution. *Astrophys. J.* **854**, 122. DOI.
- Yan, X.L., Yang, L.H., Xue, Z.K., Mei, Z.X., Kong, D.F., Wang, J.C., Li, Q.L.: 2018, Simultaneous observation of a flux rope eruption and magnetic reconnection during an X-class solar flare. *Astrophys. J. Lett.* **853**, L18. DOI.
- Zhao, M.-X., Le, G.-M., Chi, Y.-T.: 2018, Investigation of the possible source for the solar energetic particle event on 2017 September 10. *Res. Astron. Astrophys.* **18**, 74. DOI.
- Zharkova, V.V., Arzner, K., Benz, A.O., Browning, P., Dauphin, C., Emslie, A.G., Fletcher, L., Kontar, E.P., Mann, G., Onofri, M., Petrosian, V., Turkmani, R., Vilmer, N., Vlahos, L.: 2011, Recent advances in understanding particle acceleration processes in solar flares. *Space Sci. Rev.* **159**, 357. DOI.